Soft wall effects on interacting particles in billiards

H. A. Oliveira, C. Manchein, and M. W. Beims[*]

Departamento de Física, Universidade Federal do Paraná, 81531-990 Curitiba, PR, Brazil

(Received 11 June 2008; revised manuscript received 26 August 2008; published 17 October 2008)

The effect of physically realizable wall potentials (soft walls) on the dynamics of two interacting particles in a one-dimensional (1D) billiard is examined numerically. The 1D walls are modeled by the error function and the transition from hard to soft walls can be analyzed continuously by varying the softness parameter σ. For $\sigma \to 0$ the 1D hard wall limit is obtained and the corresponding wall force on the particles is the δ function. In this limit the interacting particle dynamics agrees with previous results obtained for the 1D hard walls. We show that the two interacting particles in the 1D soft walls model is equivalent to one particle inside a *soft* right triangular billiard. Very small values of σ substantiously change the dynamics inside the billiard and the mean finite-time Lyapunov exponent decreases significantly as the consequence of regular islands which appear due to the *low-energy double collisions* (simultaneous particle-particle-1D wall collisions). The rise of regular islands and sticky trajectories induced by the 1D wall softness is quantified by the number of occurrences of the most probable finite-time Lyapunov exponent. On the other hand, chaotic motion in the system appears due to the *high-energy double collisions*. In general we observe that the mean finite-time Lyapunov exponent decreases when σ increases, but the number of occurrences of the most probable finite-time Lyapunov exponent increases, meaning that the phase-space dynamics tends to be more ergodiclike. Our results suggest that the transport efficiency of interacting particles and heat conduction in periodic structures modeled by billiards will strongly be affected by the smoothness of physically realizable walls.

PACS number(s): 05.45.Ac

I. INTRODUCTION

Although physically realizable potentials are inherently soft, most billiard models used in the literature have hard walls. For example, the Sinai billiard [1], the Bunimovich stadium [2], or the Annular billiard [3], among others, have hard walls and were used successfully to study the fundamental properties of classical and quantum chaotic systems. In such models the chaotic motion of the single particle dynamics arises as the consequence of the spatial billiard geometry. The question now is about the effect and importance of physically realizable potentials on the particles dynamics inside the billiards. Some works in this direction have shown that introducing soft walls do not destroy trajectories found in the hard-wall limit [4] and may induce the appearance of regular islands in phase space [5–7]. Such regular islands inside the chaotic sea induce a "sticky" (or trapped) motion, which is a common phenomenum in conservative systems [8]. They arise from broken Kolmogorov-Arnold-Moser (KAM) [9] curves and generate a rich dynamics in quasi-integrable systems [8]. In the context of soft walls, the sticky motion has been observed theoretically and experimentally in the one particle atom-optic billiard [10,11] and has shown to affect the quantum conductance in the soft wall microwave billiard [12].

Interacting many-particles systems in soft wall billiards is the next step to be studied. Such billiards are interesting not only from the fundamental point of view in nonlinear systems [13] but also in many applications. Two recent examples can be mentioned: The effect of wall roughness in granular Poiseuille flow [14] and how the confinement of the equilibrium hard-sphere fluid to restrictive one- and two-dimensional channels with soft interacting walls modifies its structure, dynamics, and entropy [15,16]. It has been shown recently [17] that the origin of chaotic motion of two interacting particles in a one-dimensional box is due *double collisions* which occur *very close* to the hard walls. These double collisions occur when one particle is colliding with the one-dimensional (1D) wall and almost *simultaneously* collides with the other particle. As a consequence, the kind of motion generated close to the 1D walls is essential for the whole dynamics inside the billiard. Therefore we expect that the softness of the 1D walls will strongly affect the dynamics of the interacting particles.

In this contribution we generalize previous results [17,18] to the case of 1D soft walls. The equivalence between the two interacting particles in the 1D soft walls model with the motion of one particle inside a *soft* right triangular billiard is shown. In this right triangular description the role of all important parameters from the problem becomes clear. The interacting particles dynamics is studied by varying the mass ratio $\gamma = m_2 / m_1$ of the particles and the smoothness of the 1D wall potential. The reason to use the mass ratio as a dynamical parameter is related to the generation of new materials in the field of nanotechnology, where electrons may be confined inside a disk and can be affected by the surrounding material which composes the semiconductor [19]. The composition of the surrounding material changes the effective mass between particles [20,21]. We show here that a small "degree of softness (σ)" of the 1D walls, strongly decreases the mean values of the finite-time Lyapunov exponents (FTLEs). The statistics of the distributions from the FTLEs has been studied in a number of physical situations ranging from turbulent flows [22] to Hamiltonian dynamics (in many-particle system [23], and conservative mappings [24,25]). In this work we use the FTLEs distribution over initial conditions, and the
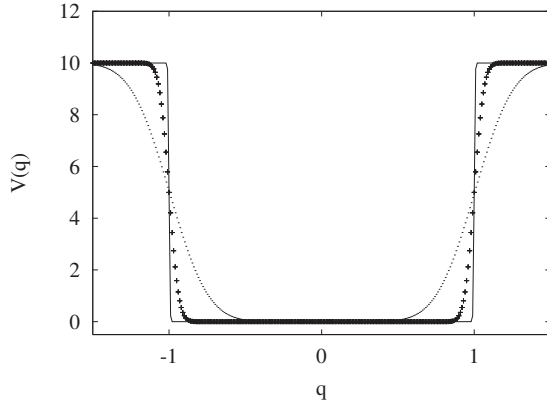
_____
[*]mbeims@fisica.ufpr.br

FIG. 1. Potential energy and corresponding forces for $F_0=10.0$ and $\sigma=5.0\times10^{-3}$ (filled line), $\sigma=5.0\times10^{-2}$ (cross points), $\sigma=9.0\times10^{-2}$ (dotted line).

number of occurrences of the most probable FTLE, which has been proposed [17] as an efficient quantity to detect small islands (dynamical traps) in phase space, to describe the qualitative and quantitative appearance of regular and sticky motion as a function of σ.

The paper is organized as follows. In Sec. II the model with soft 1D walls used in this contribution is presented. The description of this model in the right triangular is given in Sec. III. Section IV shows a systematic numerical study for the FTLEs, i.e., the number of occurrences of the most probable FTLEs as a function of the mass ratios and of the softness parameter. Poincaré surfaces of section (PSS) are used to show (a) the dynamics in the limit of hard 1D walls and (b) the rise of sticky trajectories. We end with the conclusions in Sec. V.

II. THE 1D SOFT WALLS MODEL

In this section we introduce the model used for the investigation of two interacting particles inside the 1D billiard with soft walls. This model exhibit a continuous transition between soft and hard walls. The Hamiltonian considered is

$$H = \sum_{i=1}^{2} \left[T_i + V_i(q_i) \right] + V_{int} = E, \tag{1}$$

where $T_i = \frac{p_i^2}{2m_i}$ ($i=1,2$) is the kinetic energy of particle i, $V_{int} = V_0/r$ is the Coulomb repulsion between particles with $r=|q_1-q_2|$, and $V_i(q_i)$ is the potential energy from the 1D soft walls, given by

$$V_i(q_i) = \frac{F_0}{2}\left[\text{erf}\left(\frac{q_i - d_w}{\sigma\sqrt{2}}\right) - \text{erf}\left(\frac{q_i + d_w}{\sigma\sqrt{2}}\right) \right] + F_0. \tag{2}$$

The first term on the right-hand side of Eq. (2) represents the soft 1D wall located at $q=d_w$, while the second term represents the 1D soft wall located at $q=-d_w$. Here σ is the parameter which quantifies the "softness" of the walls and F_0 is the 1D walls intensity. F_0 is added such that the total energy is positive. Figure 1 shows the potential (2) for different values of the softness parameter: $\sigma=5.0\times10^{-3}$ (filled line),

$\sigma=5.0\times10^{-2}$ (cross points), $\sigma=9.0\times10^{-2}$ (dotted line). The 1D soft walls are located at $q_w=\pm1$. As the softness parameter increases the walls become soft. An example of the 1D soft wall is shown by the dotted line in Fig. 1 for $\sigma=9.0\times10^{-2}$. As σ approaches zero (see the filled line for $\sigma=5.0\times10^{-3}$) the walls look very similar to the 1D hard walls. This limit will be called here as the 1D *quasihard* wall limit.

The corresponding left and right force of the walls on particle i is

$$F_i = \frac{1}{\sqrt{2\pi\sigma^2}}e^{-(q_i+d_w)^2/2\sigma^2} - \frac{1}{\sqrt{2\pi\sigma^2}}e^{-(q_i-d_w)^2/2\sigma^2}. \tag{3}$$

The force of the walls has the Gaussian form, which in the limit $\sigma\to0$ approaches the δ function. In this limit the corresponding potentials $V_i(q_i)$ approach the hard walls. Rescaling the time by $d\tau/dt=\sqrt{2E}$, the effective Hamiltonian of the 1D soft walls model is

$$\tilde{H} = \frac{H}{2} = \sum_{i=1}^{2}\left[\tilde{T}_i + \tilde{V}_i(q_i)\right] + \tilde{V}_{int}, \tag{4}$$

where $\tilde{V}_{int}=\tilde{V}_0/r$ and $\tilde{V}_i(q_i)$ is given by Eq. (2) by using $\tilde{F}_0$ instead F_0. The scaled potential intensities are $\tilde{V}_0=\frac{V_0}{2E}$ and $\tilde{F}_0=\frac{F_0}{2E}$. These scaled intensities show the role of the total energy on the dynamics. Results of the present work, given for a combination of the scaled parameters, are valid for other energies keeping the scaled parameters constant.

The model with smooth walls presented here differs, to our knowledge, from all models used in the literature. In our case, we assume the δ function (in the limit $\sigma\to0$) for the *force* instead for the potential, as usual. The reason to do this is simple: when we use the δ function for the *potential*, then the corresponding force is not well defined. Our model makes it possible to study the classical dynamics continuously in the transition from smooth to hard walls. Beside that, hard walls discontinuities in numerical simulations may introduce errors at each wall collision.

III. THE 1D SOFT MODEL AND THE SOFT TRIANGULAR BILLIARD

It is well know [26–28] that the motion of three particles on a frictionless ring with pointlike interactions is equivalent to one particle moving freely inside the billiard, colliding elastically with the sides of the triangle. Let us start with the Hamiltonian of the three particles on a ring, given by $H_B = \frac{p_1^2}{2m_1} + \frac{p_2^2}{2m_2} + \frac{p_3^2}{2m_3}$. We assume that the elastic collisions take place at $q_1=q_2$, $q_2=q_3$, and $q_3=q_1+1$. These collision points define the hard-wall sides of the triangle. Using the orthogonal transformation [26] ($M=m_1+m_2+m_3$):

$$q_1 = -\sqrt{\frac{m_3}{(m_1+m_2)M}}x - \frac{1}{m_1}\sqrt{\frac{m_1m_2}{(m_1+m_2)}}y + \frac{z}{\sqrt{M}},$$

$$q_2 = -\sqrt{\frac{m_3}{(m_1+m_2)M}}x + \frac{1}{m_2}\sqrt{\frac{m_1m_2}{(m_1+m_2)}}y + \frac{z}{\sqrt{M}},$$

$$q_3 = \sqrt{\frac{(m_1+m_2)}{m_3 M}}x + \frac{z}{\sqrt{M}}, \tag{5}$$

for the three particles on a ring, the resulting Hamiltonian is $H_B = \frac{1}{2}\dot{x}^2 + \frac{1}{2}\dot{y}^2 + \frac{1}{2}\dot{z}^2$. This is equivalent to the motion of one particle inside a triangular billiard with angles

$$\tan\alpha = \sqrt{\frac{m_2 M}{m_1 m_3}}, \quad \tan\beta = \sqrt{\frac{m_1 M}{m_2 m_3}}, \quad \tan\eta = \sqrt{\frac{m_3 M}{m_1 m_2}}.$$

The pointlike collision between particles 1 and 2 defines one side of the triangle at $q_1 - q_2 = 0$, and the collision of these particles with particle 3 defines the other two sides of the same triangle. For $m_3 \to \infty$ ($\eta = \pi/2$) we obtain the right triangular billiard which corresponds to the motion of two particles m_1 and m_2 moving inside the 1D box with hard walls. In this case the interaction between particles 1 and 2 is the pointlike collision and the fixed particle 3 plays the role of the 1D hard wall, kept fixed at q_3. These collisions with the 1D fixed hard wall can be represented by δ functions. However, the corresponding equations of motion are not well defined. Therefore, to describe analytically such problems we include in H_B the soft interactions between particles which, in a given limit, are expected to describe the pointlike collisions and the 1D box hard walls.

First we assume that the interaction between particles 1 and 2 is the Coulomb repulsion $V_{12} = V_{int} = V_0/|q_1 - q_2|$. In order to give an idea of the transition to hard walls in the triangle, we use the Yukawa potential $V_{12} = V_0 e^{(-|q_1-q_2|/\nu)}/|q_1 - q_2|$. The interaction between particles 1 and 2 depends only on the relative positions of both particles and $\nu > 0$ is a parameter which allows to change the interaction range from the smooth potential. For $\nu \to 0$ the limit of short interactions (pointlike collision) can be approached. Using the orthogonal transformation (5) the above interaction is written as $V_{12}(|y|) = \sqrt{\mu_{12}} V_0 e^{(-|y|/\nu\sqrt{\mu_{12}})}/(|y|)$, where $\mu_{12} = m_1 m_2/(m_1+m_2)$ is the reduced mass between particles 1 and 2. Using $V_{12}(|y|)$, the one side of the triangle located at $y=0$ is now soft, as will be shown numerically later.

Second, we assume that particles 1 and 2 interact smoothly with particle 3. In order to study the 1D box case, the location of particle 3 is kept fixed at $q_3 = \pm d_w$ and $m_3 \to \infty$. In this way particle 3 will play the role of the 1D *soft* walls. Here we consider the soft interactions $V_{i3}(x,y) = V_i(q_i)$ given by Eq. (2). Due to the soft interaction with particle 3, particles 1 and 2 can, in the ring description, interact with particle 3 on both sides, left ($q_3 = -d_w$) and right ($q_3 = +d_w$). In the limit $m_3 \to \infty$ the orthogonal transformation (5) is then reduced to the (x,y) plane

$$q_1 = -\frac{\sqrt{\mu_{12}}}{m_1}\left(y + \frac{m_1}{\sqrt{m_1 m_2}}x\right),$$

$$q_2 = \frac{\sqrt{\mu_{12}}}{m_2}\left(y - \frac{m_2}{\sqrt{m_1 m_2}}x\right). \tag{6}$$

Rescaling the time by $d\tau/dt = \sqrt{2E}$ and using the reduced orthogonal transformation (6) we obtain, after straightforward calculation, the final scaled Hamiltonian

$\widetilde{H}_B = H_B/(2E) = 1/2$ in the right triangular description [using $(\widetilde{x}, \widetilde{y}) \to (x,y)$]

$$\widetilde{H}_B = \frac{\dot{x}^2}{2} + \frac{\dot{y}^2}{2} + \widetilde{V}_{12}(|y|) + \sum_{i=1}^{2}\widetilde{V}_{i3}(x,y), \tag{7}$$

where

$$\widetilde{V}_{12}(|y|) = \widetilde{V}_0 \frac{e^{(-|y|/\sqrt{\mu_{12}}\nu)}}{|y|},$$

$$\widetilde{V}_{i3}(x,y) = \widetilde{F}_0 + \frac{\widetilde{F}_0}{2}\left\{\mathrm{erf}\left[\frac{\sqrt{2\mu_{12}}}{2m_i\sigma}\left(y + \frac{(-1)^{i+1}m_i}{\sqrt{m_1 m_2}}x\right) - \frac{\sqrt{2}d_w}{2\sigma}\right] - \mathrm{erf}\left[\frac{\sqrt{2\mu_{12}}}{2m_i\sigma}\left(y + \frac{(-1)^{i+1}m_i}{\sqrt{m_1 m_2}}x\right) + \frac{\sqrt{2}d_w}{2\sigma}\right]\right\}.$$

The total energy of the scaled problem is $\widetilde{H}_B = 1/2$ and the effect of the real energy can be seen in the scaled potential intensities $\widetilde{V}_0 = \frac{V_0\sqrt{\mu_{12}}}{2E}$ and $\widetilde{F}_0 = \frac{F_0}{2E}$. In the above Hamiltonian we observe the role of the crucial quantities of the problem, i.e., masses m_1, m_2, the softness (ν) of the interaction between particles 1 and 2, the softness (σ) of the 1D *soft* walls, and the size d_w of the 1D soft walls billiard.

Figure 2 shows the potential energy from Eq. (7) for two values of the smoothness σ, and for two values of the masses m_1 and m_2. We assume that $\widetilde{V}_{12} = \widetilde{V}_0/|y|$. First observation is that in the (x,y) plane the potential energy has a right triangle form, as expected. The left side of the triangle ($y=0$) has a smooth form due to $V_{12}(|y|)$, which is the long Coulomb repulsion between particles 1 and 2. The other two sides of the triangle (with internal angle $\eta = \pi/2$) can be soft or not, depending on σ. These two sides are equivalent to the 1D soft walls. For $\sigma = 5 \times 10^{-3}$ and $m_1 = m_2 = 1$ we nicely see in Fig. 2(a) that these two sides approach to hard walls, while for $\sigma = 0.2$ these two sides are very soft, as can be seen in Fig. 2(b). Figures 2(c) and 2(d) show the potential energy for the right triangle when the masses are changed ($m_1 = 3$ and $m_2 = 1$). Figure 2(c) for $\sigma = 5 \times 10^{-3}$ and Fig. 2(d) for $\sigma = 0.2$. Above results show us that the motion of two particle inside the 1D soft walls is equivalent to the motion of one particle inside the right triangle with soft walls.

Some limiting situations can promptly be seen from Hamiltonian (7): (a) When $F_0 = 0$ (no 1D walls) the two sides with internal angle $\eta = \pi/2$ of the triangle disappear and just the soft wall $\widetilde{V}_{12}(|y|)$ remains. The Hamiltonian is separable and integrable since the x dependence in the potential energy disappears. This means that for two interacting particle (through relative coordinates) which are not bounded inside walls, the problem is regular, as expected. (b) The kind of coupling between coordinates x and y depends on the form of the interaction used for $\widetilde{V}_{i3}(x,y)$. Therefore, these two sides (or the 1D soft walls) determine if the dynamics inside the right triangle (or inside the 1D box) is chaotic and/or regular. (c) When $m_2 \to \infty$ (or $m_1 \to \infty$) the x dependence in the argument of the error function [in $\widetilde{V}_{i3}(x,y)$] can be neglected when compared to the y dependence, and the Hamil-
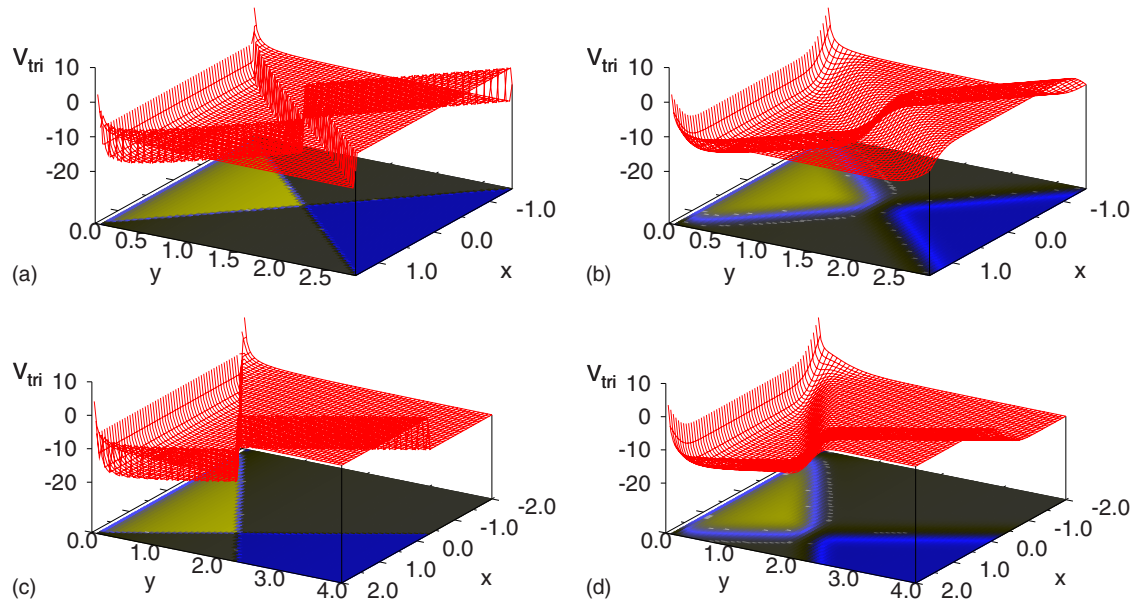
FIG. 2. (Color online) Scaled triangular potential energy (V_{tri}) from the Hamiltonian (7) with $\widetilde{F}_0=10.0$, $\widetilde{V}_0=0.5$, and $\sigma=5.0\times10^{-3}$ in (a) and (c), and $\sigma=2.0\times10^{-1}$ in (b) and (d). For (a) and (b) we have $m_1=m_2=1$, and for (c) and (d) we have $m_1=3$ and $m_2=1$.

tonian (7) is separable again. This is also an expected result, since when particle 2 (or 1) is too heavy, the motion should be regular again. (d) Increasing the billiard size d_w, the 1D soft walls come apart. The same effect is obtained by decreasing the softness σ. (d) The last limit which we would like to mention, and the most interesting one, is the hard-wall billiard case, where $\sigma\rightarrow0$ and $\nu\rightarrow0$ (and $\widetilde{V}_0\rightarrow\infty$). In this limit the whole dynamics can be explained in terms of rational and/or irrational values of α/π [28,29]. Using the Yukawa interaction in the 1D hard walls billiard, we approached this limit numerically ($\nu=0.1$) in a previous work [17], where it was also shown analytically the influence of the interaction between particles 1 and 2 to generate positive Lyapunov exponents. The softness of this interaction is essential to generate positive Lyapunov exponents, and it is possible to see that for the pointlike collisions the probability to obtain positive Lyapunov exponents goes to zero. To study this limit analytically, the interaction potentials between all particles must be chosen appropriately, and it is the subject of a future work. In this context it would be interesting to use the methodologies developed in [4–7] to study the limit $\sigma\rightarrow0$.

We finish this section by mentioning that the Hamiltonian (7) corresponds to the motion of one particle inside the right triangle suffering soft collisions at the walls. Although this is not, strictly speaking, a billiard motion as in the original sense (free particle inside a table), we will refer to it as the particle inside a soft right triangular billiard, due to the analogy shown in this section.

IV. RESULTS

We investigate the nonlinear behavior inside the 1D soft billiard by determining the distribution $P(\Lambda_t,\gamma)$ of the finite-time largest Lyapunov exponents Λ_t as a function of the mass

ratio between particles $\gamma=m_2/m_1$. This investigation was done previously for the 1D hard-wall case [17,18] and the whole dynamics depends strongly on γ. The FTLE is obtained by integrating two closed trajectories, computing the local LE after a time $\tau=0.1$ and making an average over all the local LEs. The time τ is chosen for the better convergence of the LE. We used the fourth-order Runge Kutta method with variable steps. The energy is conserved in all simulations by around 10^{-6}. For quasi-integrable system, the presence of broken KAM curves inside the chaotic sea in phase space, leads to trapping and "sticky" trajectories [8], affecting the convergence in the determination of the FTLEs, which depend now on the initial conditions. On the other hand, it implies that the distribution $P(\Lambda_t,\gamma)$, calculated over many initial conditions, contains information about the amount of regular motion (and trapped trajectories) in phase space [17,30–34]. For ergodic system and for infinite times, the Lyapunov exponents do not depend on initial conditions [35].

A. The 1D quasihard limit ($\sigma=5\times10^{-3}$)

Figure 3 shows (dashed line) the mean FTLE $\langle\Lambda_t\rangle$ as a function of the mass ratio γ for $\sigma=5\times10^{-3}$. This is the case of very small values of σ (1D quasihard wall limit) and the 1D soft walls look very similar to the 1D hard-wall potential (see Fig. 1). The mean FTLE decreases from roughly ~1.15 to 0.54 in the whole mass ratio interval. This means that the dynamics is becoming more and more regular, as expected, since $\gamma\rightarrow\infty$ constitutes an integrable limit with the heavy particle at rest. However, at $\gamma\sim1.0$ the mean FTLE increases, showing that the symmetry for equal masses increases the amount of irregular motion. Figure 3 also shows (full line) results for the case of hard 1D walls, published previously [18]. In that case, and therefore in the case observed here, the peak at $\gamma=1.0$ is the consequence of the
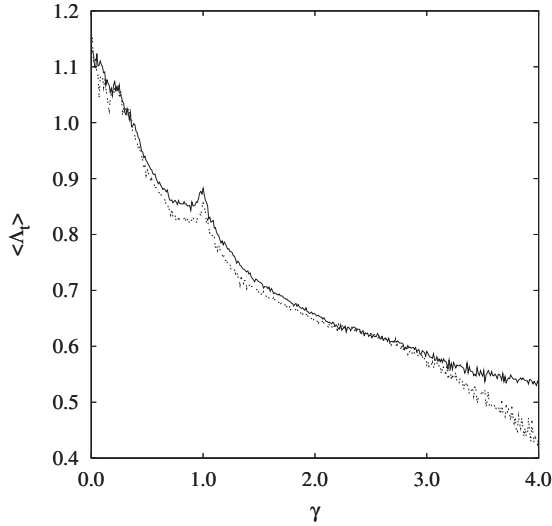
FIG. 3. Mean values of the finite-time largest Lyapunov exponent calculated over 200 trajectories up to time $t = 10^4$ and at scaled energy $\tilde{E} = 0.5$, $\tilde{V}_0 = 1.0$, $\tilde{F}_0 = 10.0$, for $\sigma = 5 \times 10^{-3}$ (dashed line). This is the 1D quasihard wall limit. For comparison, the full line shows results obtained for the 1D hard walls [18]. For each trajectory the largest FTLE is evaluated over 10^5 samples.

resonance observed in the limit of hard-point collisions between particles. The qualitative behavior of the FTLEs could be explained in [18] with the help of some special periodic orbits from the Gauss map. For the purpose of this work we can observe that both curves in Fig. 3 are in good agreement. This confirms that the model of 1D soft walls presented here reproduces correctly, in the limit $\sigma \rightarrow 0$, the 1D hard wall case. However, small differences can be observed in Fig. 3 for $\gamma \lesssim 0.4$, $\gamma \sim 0.96$, and $\gamma \gtrsim 3.0$. These differences will be explained later, where we also show some Poincaré surfaces of section (PSS) and discuss more details of the whole dynamics for different values of the mass ratio.

To analyze deeper the effect of the smooth potential on the particles dynamics, Fig. 4 shows the finite-time distribution of the largest Lyapunov exponent, $P(\Lambda_t, \gamma)$, for the (a) 1D quasihard wall limit $\sigma = 5 \times 10^{-3}$ and (b) the 1D hard wall case from [18]. The gray points below the main curve are related to chaotic trajectories which were trapped for a while close to regular islands. Since both figures are quite similar, the 1D quasihard limit also represents adequately the 1D hard wall case concerning trapped trajectories. An interesting feature in Fig. 4 is the change of the width of $P(\Lambda_t, \gamma)$ around the number of occurrences of the most probable Λ_t^p defined through [17]

$$\left. \frac{\partial P(\Lambda_t, \gamma)}{\partial \Lambda_t} \right|_{\Lambda_t = \Lambda_t^p} = 0. \tag{8}$$

For mass ratios close to $\gamma \sim 1.0$, for example, many initial condition lead to different values of Λ_t. In this region, Λ_t^p has a minimum as a function of γ, which is a clear demonstration of the presence of "sticky" trajectories.

To determine the amount of "sticky" and regular trajectories in phase space we follow Λ_t^p as a function of the mass
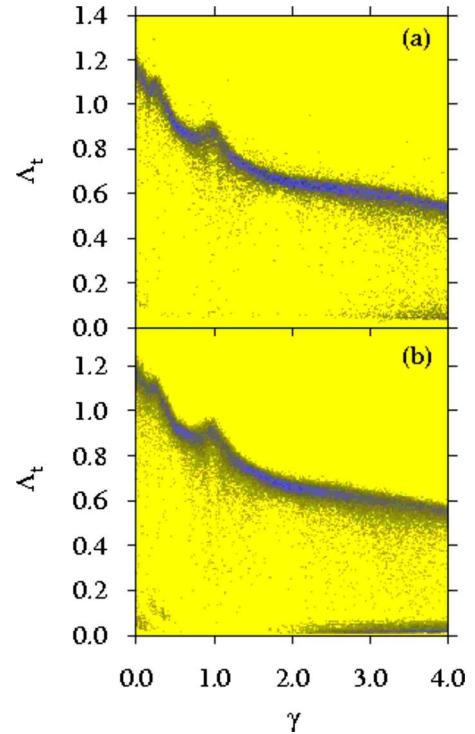

FIG. 4. (Color online) Finite-time distribution of the largest Lyapunov exponent $P(\Lambda_t, \gamma)$ calculated over 200 trajectories up to time $t = 10^4$, for (a) 1D quasihard wall limit $\sigma = 5 \times 10^{-3}$, and (b) 1D hard wall limit from [18]. With increasing $P(\Lambda_t, \gamma)$ the color changes from light to dark (white over yellow and blue to black).

ratio γ. In fact, we follow $P(\Lambda_t^p)$, which is the normalized number of occurrences of the most probable LE, or the probability to obtain Λ_t^p. This is shown in Fig. 5. When $P(\Lambda_t^p)$ is large, a large fraction of initial conditions lead to the same Λ_t and trapped trajectories are rare. For example, the maximum of $P(\Lambda_t^p)$ in Fig. 5(a) [and Fig. 5(b)] close to $\gamma \sim 1.8$, is the region in Fig. 4(a) where gray points below the main curve are rare. On the other hand, close to $\gamma \sim 0.96$ we have a minimum in Fig. 5(a) [and Fig. 5(b)], which is the consequence of the large dispersion around $\gamma \sim 0.96$ in Fig. 4(a). Again the quasihard limit [Fig. 5(a)] and hard wall [Fig. 5(b)] agree very well. The fast variation of $P(\Lambda_t^p)$ is due to statistical fluctuations in its determination over initial conditions.

Figure 6 shows the PSS for $\gamma = 1.0, 1.8$ and compares the 1D quasihard limit [Figs. 6(a) and 6(b)] with the 1D hard wall case [Figs. 6(c) and 6(d)]. Both cases are alike. The PSS is constructed in the following way: each time particle 2 is located at the origin, and $p_2 > 0.0$, then the point (q_1, p_1) is recorded. Since this work is focused on the dynamics inside the realistic 1D box problem, we have chosen to present results of the PSS in the 1D box coordinates, instead in the right triangular coordinates (x, y). In fact, we have checked some PSS in the (x, y) coordinates and no additional relevant informations for the present work were obtained. It can be observed in Fig. 6 that for $\gamma = 1.8$ the PSS is almost filled with the chaotic trajectory, while for $\gamma = 1.0$ some regular islands and forbidden trajectories appear which induce the trapping trajectories (these trapped trajectories cannot be
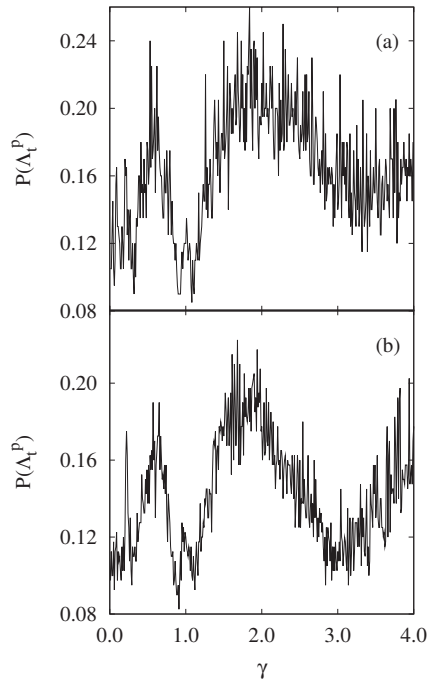
FIG. 5. Normalized values of the most probable Lyapunov exponent Λ_t^p for (a) 1D quasihard case $\sigma=5\times10^{-3}$ and (b) 1D hard wall case from [18].

seen in the resolution used in Fig. 6). Therefore, in addition to the mean FTLE and the number of occurrences of the FTLE, also in the PSSs the quasihard limit and the hard 1D wall case are almost identical, showing that our soft model correctly describes the hard 1D wall limit $\sigma\to0$. This will change drastically next, when the softness parameter increases.
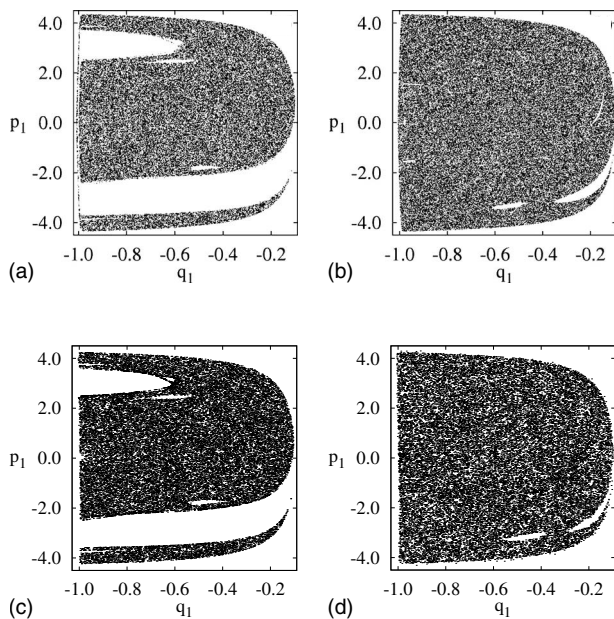

FIG. 6. Poincaré surfaces of section for particle 1 and (a), (b) 1D quasihard limit and (c), (d) 1D hard wall case. (a), (c) $\gamma=1.0$, and (b), (d) $\gamma=1.8$.
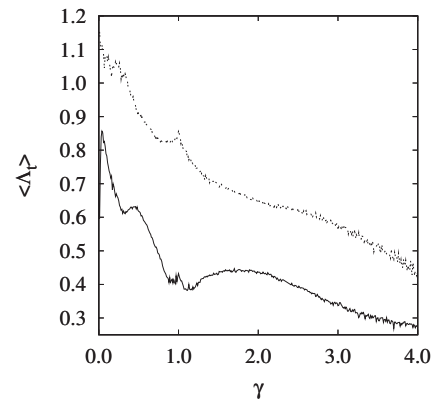

FIG. 7. Mean values of the finite-time largest Lyapunov exponent calculated over 400 trajectories up to time $t=10^4$ and at scaled energy $\tilde{E}=0.5$, $\tilde{V}_0=1.0$, $\tilde{F}_0=10$ for the 1D soft wall with $\sigma=5\times10^{-2}$ (full line). For comparison, the full line shows results obtained for the quasi-hard 1D wall from Fig. 3. For each trajectory the largest FTLE is evaluated over 10^5 samples.

B. The 1D soft case $\sigma=5\times10^{-2}$

Finally we discuss the case of 1D soft walls. The form of the 1D wall potential is shown in Fig. 1 (see cross points for $\sigma=5\times10^{-2}$). Although the value of σ is small, the effect on the particles dynamics is astonishing. Figure 7 shows the mean values of the finite-time largest Lyapunov exponents for $\sigma=5\times10^{-2}$ (full line) compared with the quasihard 1D wall limit (dashed line) from Fig. 3. The effect of the small soft potential is remarkable. The mean FTLEs decrease around 50% and the peak observed close to $\gamma=1.0$ (full line) is now a minimum. A minimum also appears close to $\gamma\sim0.40$.

To understand better what happens, Fig. 8(a) shows the finite-time distribution of the largest Lyapunov exponent for this case. Clearly we see that, although the peak close to $\gamma=1.0$ still exist, the dispersion around the most probable FTLE is very large. This large dispersion affects the mean Lyapunov exponents from Fig. 3 and a minimum occurs at $\gamma=1.0$. This strong dispersion around $\gamma=1.0$ is also confirmed by the accentuated minimum of the number of occurrences of the most probable FTLE plotted in Fig. 8(b). A similar effect, but with smaller intensity occurs for $\gamma\sim0.4$. The mean FTLEs increase as γ decreases, the amount of gray points below the main curve increases and the number of occurrences of the most probable FTLE also decreases.

Many other values of the mass ratio γ could be discussed to analyze the appearance of island in phase space. Instead of doing so we would like to show some PSS in order to discuss the dynamics of the interacting particles in the 1D soft walls. We start by showing the case of $\gamma=1.0$, for which many trapped trajectories and islands are expected. Figure 9(a)–9(c) shows the corresponding PSS. Since for the PSS we used the condition $p_2>0.0$, particle 2 is always moving to the right at $q_2=0$. Because the interaction between particles is repulsive, we expect that particle 1 crosses the PSS a distinct number of times for $p_1<0.0$ than for $p_1>0.0$. This physical effect is the origin of the asymmetry in Fig. 9(a) observed in p_1. Additionally, due to $p_2>0.0$, trajectories on
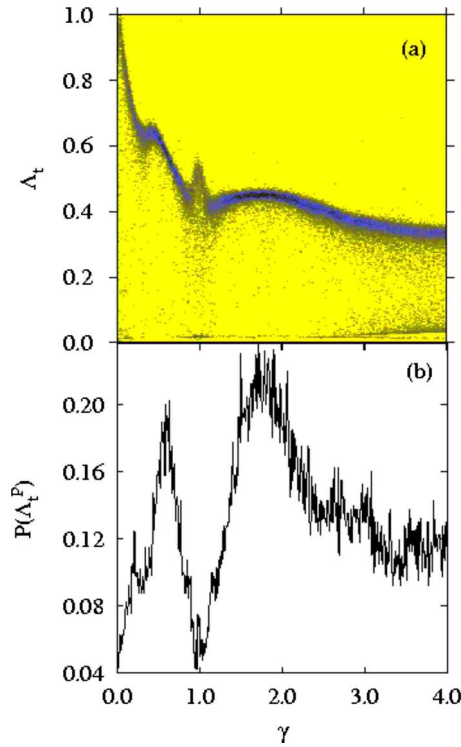
FIG. 8. (Color online) (a) Finite-time distribution of the largest Lyapunov exponent $P(\Lambda_t, \gamma)$ calculated over 400 trajectories up to time $t = 10^4$, $\sigma = 5 \times 10^{-2}$. With increasing $P(\Lambda_t, \gamma)$ the color changes from light to dark (white over yellow and blue to black); (b) corresponding normalized number of occurrences of the most probable Lyapunov exponent Λ_t^p.

the PSS with negative momentum ($p_1 < 0.0$) are less affected by particle 2 than trajectories with $p_1 > 0.0$. Since the chaotic motion results from the simultaneous effect of the 1D walls and the mutual interactions, we conclude that trajectories with
$p_1 < 0.0$ should be more regular. Therefore we expect more island for $p_1 < 0.0$ than for $p_1 > 0.0$ [see Fig. 9(a)]. Observe that for $p_1 < 0.0$ the islands extend themselves from $q_1 \sim -1.0$ until $q_1 \sim -0.1$, which is very close to particle 2, located at $q_2 = 0$. For $p_1 > 0$ the interval of islands goes from $q_1 \sim -1.0$ until $q_1 \sim -0.4$, very far from particle 2. Close to the left 1D wall ($q_1 \sim -1.0$), the momentum of particle 1 remains in the interval $-1.0 \lesssim p_1 \lesssim 1.0$, while close to particle 2 ($q_1 \sim -0.1$) we have chaotic trajectories with essentially only positive momenta ($0.0 \lesssim p_1 \lesssim 1.0$) due the repulsion of particle 2. For $-1.0 \lesssim p_1 \lesssim 0.0$ we have essentially regular

trajectories since both particles are moving apart. The main island in Fig. 9(a) is related to the following *regular trajectory*: particle 1 is moving to the left with a small momentum which does not allow it to "penetrate" very much the 1D soft wall. It "collides" with the 1D soft wall and simultaneously is affected by the interaction force with magnitude comparable to the magnitude of the 1D wall force. This is called here as the *low-energy double collision*, which in this example occurs between particle 1 (low momentum), particle 2, and the 1D soft wall. After colliding with the left 1D wall, particle 1 moves to the right with a small momentum and cannot approach particle 2 very much due to the long Coulomb repulsion. Subsequently it changes its direction and goes back to the left 1D wall.

Another interesting property occurs very close to the "top of the 1D soft wall potential." We call the readers attention to the fact that "top of the 1D soft wall potential" in our one-dimensional billiard is the closest point that particles approach the turning point. In other words, it is the point where the "penetration" into the soft 1D wall is maximal. When particle 1 has enough momentum ($p_1 = -4.0$) to "climb" ("penetrate") the left 1D wall until the "top," it reaches the turning point on the left (around $q_1 \sim -1.1$) with zero momenta [see Fig. 9(a)]. After that, particle 1 returns to move to the right, accelerates ($p_1 = +4.0$) and travels until the other extremum at $q_1 \sim -0.2$. This is a nonperiodic *chaotic trajectory* with a behavior similar to the regular trajectory discussed above. The main difference is that the regular trajectory has not enough momentum to "climb" ("penetrate") the 1D wall potential until the "top." In this example of the chaotic trajectory, the *high-energy double collision* occurs between particle 1 (high momentum), particle 2, and the soft 1D wall. It is worth it to mention that in the triangle description the above high- and low-energy double collisions correspond to the high- and low-energy particle collisions with the corners of the triangle which are located at $y = 0$.

Figures 9(b) and 9(c) show a magnification of some regular regions from Fig. 9(a), revealing the existence of the regular islands. Figure 9(d) shows the PSS for $\gamma = 0.8$, which compared to $\gamma = 1.0$ presents a small number of islands. This is in agreement with results from Fig. 8(b), where the number of occurrences of the most probable FTLE has not a minimum for $\gamma \sim 0.8$, and a small number of trapped trajectories is expected.

We conclude this section by saying that the softness of the 1D wall decreases the mean FTLE. This effect is so strong that it is responsible for the small differences observed for $\gamma \lesssim 0.4$, $\gamma \sim 0.96$, and $\gamma \gtrsim 3.0$ between the quasihard limit
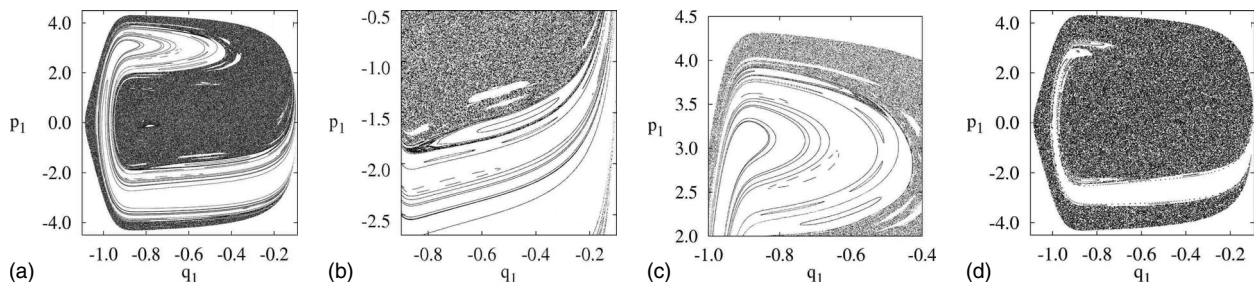

FIG. 9. Poincaré surfaces of section for $\sigma = 5 \times 10^{-2}$ and for (a) $\gamma = 1.0$, and their magnification (b) and (c). Figure (d) is for $\gamma = 0.8$.
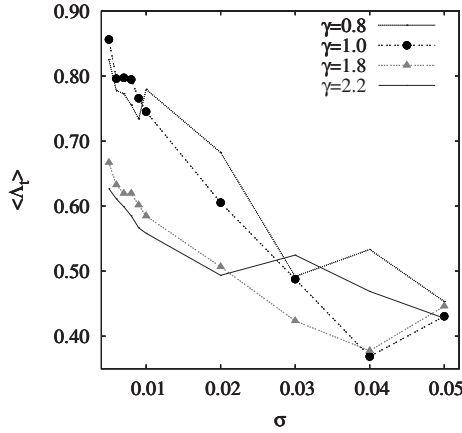
FIG. 10. Mean values of the finite-time largest Lyapunov exponent calculated over 400 trajectories up to time $t = 10^4$ as a function of σ, for $\gamma = 0.8, 1.0, 1.8, 2.2$.

FIG. 11. Normalized number of occurrences of the most probable Lyapunov exponent Λ_t^p as a function of σ.

and the hard wall case [see Fig. 3]. For these values of γ the number of occurrences of the FTLE from Fig. 5 has a minimum, and a larger amount of sticky trajectories is expected. This means that the softness of the 1D wall has a stronger influence on space phases with sticky trajectories. In addition we note that the above differences are stronger for $\gamma \gtrsim 3.0$ [see Fig. 3]. This can be nicely explained using properties of the particle-particle frontal collision case. When a frontal collision of the particles occurs, then for $\gamma = m_2/m_1 > 3.0$ the momentum of particle 2 is large enough and, after one collision, it continuous to move in the same direction as before the collision. Obviously this depends on the particles energy, but in average, more frontal collisions are necessary to change the direction of movement of particle 2 when $\gamma > 3.0$. This property increases the amount of double collisions close to the 1D wall, and consequently, the effect of the 1D soft wall is more pronounced when $\gamma > 3.0$, and the dynamics becomes more regular when compared to the 1D hard wall case.

C. Dependence on the softness parameter σ

In this section we analyze the mean FTLEs, $\langle \Lambda_t \rangle$, and the number of occurrences of the most probable FTLEs as a function of the parameter σ. All simulations were realized over 400 initial conditions and for the mass ratios $\gamma = 0.8, 1.0, 1.8, 2.2$. Figure 10 shows $\langle \Lambda_t \rangle$ for ten different values of σ in the interval $5 \times 10^{-3} \leqslant \sigma \leqslant 5 \times 10^{-2}$. This is exactly the transition region between the 1D quasihard limit and the 1D soft wall. We observe that the main behavior for all mass ratios is that the mean FTLEs decrease as σ increases. This means that the degree of chaoticity decreases when the softness of the 1D wall increases.

Figure 11 shows the number of occurrences of the most probable FTLE as a function of σ for the values of γ shown in Fig. 10. For all mass ratios, but one (see filled circles $\gamma = 1.0$), $P(\Lambda_t^p)$ increases with σ. This means that the dispersion around the most probable FTLE decreases when σ increases, i.e., many initial conditions converge to the same Lyapunov exponent, and a more ergodiclike motion is ex-
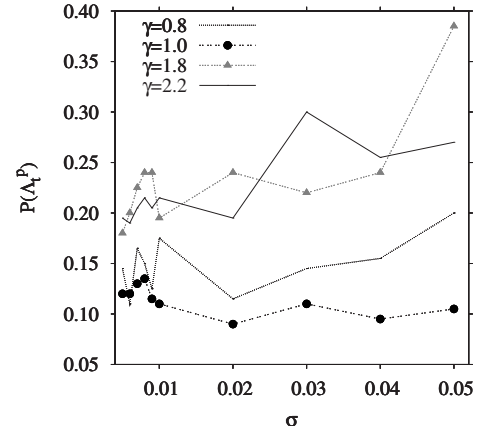
pected when compared with other mass ratios. This is interesting seeing that for higher values of σ the degree of chaoticity decreases but the dynamics becomes more ergodiclike. Compare for example the values of $P(\Lambda_t^p)$ in Fig. 11 for $\sigma = 5 \times 10^{-2}$ and $\gamma = 0.8, 1.0$. For $\gamma = 0.8$ we have $P(\Lambda_t^p) \sim 0.2$, and for $\gamma = 1.0$ we have $P(\Lambda_t^p) \sim 0.1$. So we expect that the dynamics is more ergodiclike for $\gamma = 0.8$. This really happens and can be confirmed visually comparing Figs. 9(a) and 9(d). Clearly the amount of regular island inside the chaotic sea is smaller for $\gamma = 0.8$ [Fig. 9(d)] than for $\gamma = 1.0$ [Fig. 9(a)].

V. CONCLUSIONS

To conclude, we discuss the effect of physical realizable potentials (soft potentials) on the dynamics of interacting particles inside 1D billiards. This contribution generalizes previous results [17,18] to the case of 1D soft walls. The 1D soft walls are modeled by the error function with the softness parameter σ. In the limit $\sigma \to 0$ the 1D wall force on the particle is given by the δ function. This allows us to study continuously the dynamics of interacting particles in the transition from soft to hard walls. The equivalence between the two interacting particles in the 1D soft walls model with the motion of one particle inside a *soft* right triangular billiard is shown. The role of all parameters from the model becomes clear in the right triangular description. Since the chaotic motion of interacting particles inside 1D billiards is generated by double collisions which occurs close to the 1D walls [17], we expect the influence of the soft 1D walls on the particles dynamics to be very strong. Using the mean FTLE and the number of occurrences of the most probable FTLE, we analyze the dynamics of the interacting particles when the softness parameter changes from the 1D quasihard limit ($\sigma = 5 \times 10^{-3}$) to the 1D soft wall case ($\sigma = 5 \times 10^{-2}$). We show that the 1D quasihard wall limit agrees very well with results from the 1D hard wall case, analyzed previously [18]. When the softness parameter increases to $\sigma = 5 \times 10^{-2}$, the mean FTLEs decreases substantiously (around 50%) when compared to the FTLEs from $\sigma = 5 \times 10^{-3}$. Although both 1D walls are visually very similar, the dynamics of the interacting particles changes considerably. While regular is-

lands and trapped trajectories are induced by the *low-energy double collisions*, the chaotic motion is produced by the *high-energy double collisions*. Double collisions are characterized by the simultaneous particle-particle-1D wall collisions. The rise of trapped trajectories is shown by using the number of occurrences of the most probable FTLE and the corresponding PSS.

Results from the present paper strongly suggest that the transport of interacting particles and heat conduction in physical devices [10–12,36–40], which can be described by open billiard models, will substantiously be affected by physically realizable wall potentials (soft walls). In such models, particles (heat) are injected at one open end of the billiard, and the efficiency of the transport depends on how long (among other properties) particles (heat) will need to reach the other open end of the billiard. Therefore, trapped trajectories induced by the soft walls *and* interacting particles, as shown in this paper, may substantiously increase the time spend by the particles (heat) inside the soft billiard, affecting the transport efficiency.

[1] Y. G. Sinai, Funct. Anal. Appl. **2**, 61 (1968).

[2] L. A. Bunimovich, Funct. Anal. Appl. **8**, 254 (1974).

[3] O. Bohigas, D. Boosé, R. E. de Carvalho, and Marvulle, Nucl. Phys. A **560**, 197 (1993).

[4] A. Rapoport, V. Rom-Kedar, and D. Turaev, Commun. Math. Phys. **272**, 567 (2007).

[5] D. Turaev and V. Rom-Kedar, Nonlinearity **11**, 575 (1998).

[6] V. Rom-Kedar and D. Turaev, Physica D **130**, 187 (1999).

[7] D. Turaev and V. Rom-Kedar, J. Stat. Phys. **112**, 765 (2003).

[8] G. M. Zaslavsky, Phys. Rep. **371**, 461 (2002).

[9] A. J. Lichtenberg and M. A. Lieberman, *Regular and Chaotic Dynamics* (Springer-Verlag, Berlin, 1992).

[10] A. Kaplan, N. Friedman, M. Andersen, and N. Davidson, Phys. Rev. Lett. **87**, 274101 (2001).

[11] A. Kaplan, N. Friedman, M. Andersen, and N. Davidson, Physica D **187**, 136 (2004).

[12] B. Weingartner, S. Rotter, and J. Burgdörfer, Phys. Rev. B **72**, 115342 (2005).

[13] V. J. Donnay, J. Stat. Phys. **96**, 1021 (1999).

[14] K. C. Vijayakumar and M. Alam, Phys. Rev. E **75**, 051306 (2007).

[15] J. Mittal, J. R. Errington, and T. M. Truskett, Phys. Rev. Lett. **96**, 177804 (2006).

[16] J. Mittal, J. R. Errington, and T. M. Truskett, J. Chem. Phys. **126**, 244708 (2007).

[17] M. W. Beims, C. Manchein, and J. M. Rost, Phys. Rev. E **76**, 056203 (2007).

[18] C. Manchein and M. W. Beims, Chaos, Solitons Fractals (in press).

[19] M. A. Reed and W. P. Kirk, *Nanostructure and Fabrication* (Academic Press, Boston, 1989).

[20] O. Gunawan, Y. P. Shkolnikov, E. P. DePoortere, E. Tutuc, and M. Shayegan, Phys. Rev. Lett. **93**, 246603 (2004).

[21] U. Merkt, J. Huser, and M. Wagner, Phys. Rev. B **43**, 7320 (1991).

[22] D. Beigie, A. Leonard, and S. Wiggins, Phys. Rev. Lett. **70**, 275 (1993).

[23] C. Amitrano and R. S. Berry, Phys. Rev. Lett. **68**, 729 (1992).

[24] M. A. Sepúlveda, R. Badii, and E. Pollak, Phys. Rev. Lett. **63**, 1226 (1989).

[25] J. D. Szezech, S. R. Lopes, and R. L. Viana, Phys. Lett. A **335**, 394 (2005).

[26] G. Casati and T. Prosen, Phys. Rev. Lett. **83**, 4729 (1999).

[27] S. L. Glashow and L. Mittag, J. Stat. Phys. **87**, 937 (1996).

[28] R. Artuso, G. Casati, and I. Guarneri, Phys. Rev. E **55**, 6384 (1997).

[29] G. Casati and J. Ford, J. Comput. Phys. **20**, 97 (1976).

[30] P. Grassberger, R. Badii, and A. Politi, J. Stat. Phys. **51**, 135 (1988).

[31] E. J. Kostelich, I. Kan, C. Grebogi, E. Ott, and J. A. Yorke, Physica D **109**, 81 (1997).

[32] H. Schomerus and M. Titov, Phys. Rev. E **66**, 066207 (2002).

[33] M. Falcioni, U. M. B. Marconi, and A. Vulpiani, Phys. Rev. A **44**, 2263 (1991).

[34] S. Tomsovic and A. Lakshminarayan, Phys. Rev. E **76**, 036207 (2007).

[35] V. I. Oseledec, Trans. Mosc. Math. Soc. **19**, 197 (1968).

[36] A. Barreiro, R. Rurali, E. R. Hernandez, J. Moser, T. Pichler, L. Forro, and A. Bachtold, Science **320**, 775 (2008).

[37] B. Li, L. Wang, and G. Casati, Phys. Rev. Lett. **93**, 184301 (2004).

[38] G. Casati, C. Mejia-Monasterio, and T. Prosen, Phys. Rev. Lett. **98**, 104302 (2007).

[39] L. Wang, G. Benenti, G. Casati, and B. Li, Phys. Rev. Lett. **99**, 244101 (2007).

[40] G. Casati, C. Mejia-Monasterio, and T. Prosen, Phys. Rev. Lett. **101**, 016601 (2008).